JOURNAL OF CATALYSIS **173,** 295–303 (1998)
ARTICLE NO. CA971949

Investigation of Pt/γ-Al_2O_3 Catalysts Prepared by Sol–Gel Method

XAFS and Ethane Hydrogenolysis

Ihl Hyun Cho,* Seung Bin Park,*,[1] Sung June Cho,† and Ryong Ryoo†

*Department of Chemical Engineering, †Department of Chemistry, Center for Molecular Science, Korea Advanced Institute of Science and Technology, 373-1 Kusong-dong Yusong-gu Taejon 305-701 Korea

Received January 6, 1997; revised August 12, 1997; accepted October 23, 1997

The physical and chemical properties of alumina-supported Pt prepared by sol–gel method were investigated using BET surface area measurement, hydrogen chemisorption, transmission electron microscopy, X-ray powder diffraction, and X-ray absorption fine structure (XAFS). The BET surface area, pore size, and pore volume of Pt/γ-Al_2O_3 obtained from sol–gel method were similar to those of impregnated catalysts. The result of XAFS showed that the platinum particles consisted of 20 atoms, ca 1 nm, independent of the preparation method. However, the available metal surface area in the sol–gel catalysts for hydrogen chemisorption decreased by as much as 30%, compared to the impregnated catalyst. The turnover frequency of ethane hydrogenolysis reaction was considerably lower than that of the impregnated catalyst. Thus, we concluded that the platinum particles in the Pt/γ-Al_2O_3 sol–gel catalysts were buried in the γ-Al_2O_3. This burial of particles was the cause of a strong metal support interaction and resulted in high sintering resistance of metal particles at 873 K in air.

INTRODUCTION

In general, alumina-supported Pt catalysts have been prepared either by impregnation or by ion-exchange method. Recently, the sol–gel method was proposed as a new preparation method of supported metal catalyst (1–3). The sol–gel catalyst was prepared from a homogenous solution containing both the metal precursors and the support precursors. The sol-gel catalyst showed a high dispersion (4–6), a high thermal resistance to sintering (7–9), and a low deactivation rate (10–12), compared with the conventional impregnated catalysts.

In conventional impregnated catalysts, the active components are present on the surface of the support. However, sol–gel catalysts can have various distributions of active component over the support. For example, the active component can be incorporated into the framework of the support (10–12, 15–20) or partially buried at the surface of the support (13, 14). Catalytic behavior of the silica-supported metal catalysts obtained through the sol–gel method has been investigated by many researchers. Lopez *et al.* (9–21) added tetraethyl orthosilicate (TEOS) in a dropwise fashion to a mixture of $H_2PtCl_6 \cdot xH_2O$, ethanol, and water. Analysis of the resulting catalyst showed a disagreement in the particle size when measured by transmission electron microscopy (TEM) and hydrogen chemisorption. The discrepancy is suggested to be due to the incorporation of Pt particles into the framework of the support. On the contrary, Gonzalez *et al.* (22) claimed that the platinum particles in the Pt/SiO_2 catalysts were not occluded in the silica matrix. They suggested that the Pt dispersion was much lower in their Pt/SiO_2 catalyst due to a weak interaction between the metal precursor and the support precursor (21, 22). Therefore, precise measurement of particle size is necessary to clarify the particle morphology and its effect.

In the present work, X-ray absorption fine structure (XAFS), transmission electron microscopy (TEM), powder X-ray diffraction (XRD), and hydrogen chemisorption were used to investigate if the platinum metal particles obtained from the sol–gel method are occluded into the γ-Al_2O_3. Ethane hydrogenolysis was also performed over the Pt/γ-Al_2O_3 sol–gel catalyst to elucidate the effect of particle morphology on the catalytic activity.

EXPERIMENTAL

Catalyst Preparation

The preparation procedure of alumina-supported platinum catalysts by sol–gel method is shown in Fig. 1. First, AIP (Junsei, 99%) was hydrolyzed at 358 K for 30 min with water to AIP mole ratio of 100. This solution was then peptized by adding HNO_3 (Junsei, HNO_3/AIP = 0.2 mol ratio). The pH of the solution was found to be 4.2 after HNO_3 was added. This peptization produced the transparent aluminum monohydroxide sol. A second solution was

[1] To whom correspondence should be addressed. E-mail: sbpark@hanbit.kaist.ac.kr.

0021-9517/98 $25.00

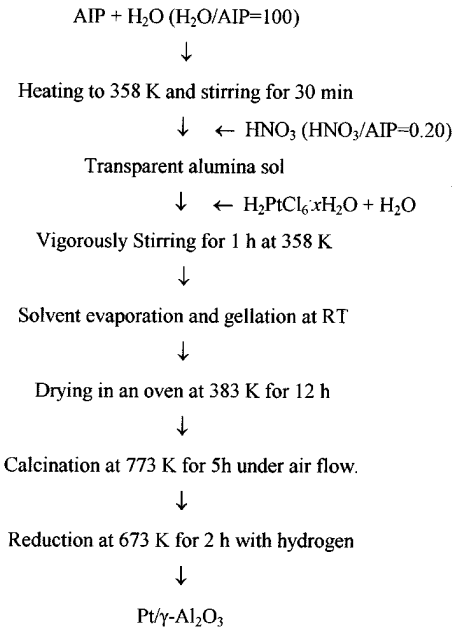

FIG. 1. Schematic flow chart for the preparation of Pt/γ-Al_2O_3 by sol–gel method.

prepared by dissolving $H_2PtCl_6 \cdot xH_2O$ (Aldrich, 99.9%) dissolved in water. This Pt salt solution was added to the AIP-derived alumina sol at 358 K and the mixture was vigorously stirred for 1 h. The alcoholic solvent was removed by drying at room temperature for 24 h. A rigid solid was formed after the solvent removal. The resulting solid was dried at 383 K for 12 h in an oven, followed by calcination under air flow in a crucible (30 ml high form porcelain). The airflow rate was 2 L min^{-1} g^{-1}. The temperature was linearly increased from room temperature to 773 K over 10 h and then maintained at 773 K for 2 h. The resulting catalyst was denoted Pt-*x*-SG-*yyy*, where *x* and *yyy* were the Pt content and the stage of heat treatment, and SG indicates that the catalysts are prepared by the sol–gel method.

The Pt/γ-Al_2O_3 catalysts were also prepared by a conventional impregnation method. An aqueous solution of $H_2PtCl_6 \cdot xH_2O$ was impregnated into alumina, which was prepared by the sol–gel method. The other preparation conditions were the same as above. The resulting catalyst was denoted Pt-*x*-IM-*yyy*, where IM indicates that the catalysts are prepared by impregnation method. The metal content of Pt/γ-Al_2O_3 samples was analyzed using inductively coupled plasma (ICP1000III, Shimadzu) spectroscopy.

The calcined Pt/γ-Al_2O_3 was reduced by H_2 flow (99.999%, passed through a MnO/SiO_2 trap) in a Pyrex U-tube flow reactor. The H_2 flow rate was 200 ml min^{-1} g^{-1}, and the reduction temperature was linearly increased to 673 K over 4 h and maintained at 673 K for 2 h. The reduced sample was followed by evacuation under a pressure of 1×10^{-5} Torr at 673 K for 2 h to remove chemisorbed hydrogen. The prepared sample was transferred to an adsorption cell, which was attached to the Pyrex U-tube flow reactor, and then the adsorption cell was sealed off by flame and used for hydrogen chemisorption. The catalyst sintering was performed on the reduced Pt/γ-Al_2O_3 catalysts in airflow at 873 K for 20 h. The final sintering temperature was reached at 10 K min^{-1}. The sample was cooled down to room temperature and subsequently reduced in H_2 at 673 K for 2 h.

Catalyst Characterization

The local structure around the platinum in each preparation step was investigated by XAFS spectroscopy. X-ray absorption of the solution sample was measured using a specially designed cell with Kapton windows (125 μm, DuPont) which was glued with Torr Seal (Varian). Thickness of the cell was adjusted in order to obtain optimal signals. The dried and sintered sample was pasted on the adhesive tape (3M tape) in ambient air.

For the *in-situ* XAFS measurement, the powder sample about 0.10–0.20 g was pressed into a self-supporting wafer 10 mm in diameter. The sample wafer was pretreated using a Pyrex U-tube reactor that was joined to an XAFS cell. The XAFS cell had Kapton windows which were joined using a Torr Seal. After the sample was transferred into the XAFS cell, the sample in the cell was sealed off by flame in flowing either H_2 or O_2. The X-ray absorption spectra of Pt L_{III} edge was measured using a Si(311) monochrometer on the Beam Line 10B station at the Photon Factory in Tsukuba. Injection beam energy was 2.5 GeV and ring current was 250–350 mA. The X-ray absorption at Pt L_{III} edge was obtained at room temperature in a transmission mode. The intensity of incident and transmitted X-rays were measured using an ionization chamber filled with 15% Ar + 85% N_2 and 100% Ar, respectively.

Analysis of the X-ray absorption data was carried out with a standard method using UWXAFS2 program package (23) and FEFF 6.0 distributed by University of Washington (24, 25).

Total surface area and pore size measurements were performed using a Micromeritics ASAP 2400. Total surface areas were obtained by N_2 physisorption at its saturation pressure. The pore size distributions were obtained from the desorption branch of the isotherm.

XRD patterns were collected using a RIGAKU D/MAX-RB equipped with Cu Kα X-ray source. The 2θ region of 10–70° was scanned with a rate of 4° min^{-1}.

Pt metal particle size was measured by using a Philips EM20 instrument. A small portion consisting of a 10-mg sample was suspended in ethanol. The ethanol suspension was sonicated for 1 min. The carbon-coated 200-mesh copper grid was dipped into the sonicated suspension and allowed to dry at room temperature.

The platinum dispersion was measured hydrogen backsorption method or H_2–O_2 titration method. The adsorption temperature was controlled at 298 ± 0.1 K by a constant temperature circulation bath. The H_2–O_2 titration was performed as proposed by Benson and Boudart (26). The pretreated Pt/γ-Al_2O_3 sample was first exposed to the oxygen for 1 h at 1 atm. After evacuation of sample for 1 h to remove weakly adsorbed oxygen atoms, the hydrogen chemisorption was measured over a pressure range 5–50 kPa.

Catalytic Activities

The ethane hydrogenolysis reaction over Pt/γ-Al_2O_3 was conducted using a continuous Pyrex U-tube reactor at atmospheric pressure. Before a catalytic activity test, sol–gel samples were ground and then sieved through 100 mesh. A 0.3-g sample was re-reduced by H_2 flow (99.999%, passed through a R&D oxygen/moisture trap), because the sample was open to air at room temperature after the chemisorption measurement. The flow rate of H_2 was 200 ml min^{-1} g^{-1}, and the reduction temperature was linearly increased to 673 K over 2 h and maintained at 673 K for 2 h. After reduction, the ethane hydrogenolysis reaction was started by introducing ethane and hydrogen into the reactor. Helium was used to dilute the gas. The partial pressure of ethane and hydrogen were 6 and 33 kPa, respectively. The total flow rate ($H_2 + C_2H_6 + He$) was 60 ml min^{-1}. In our experimental conditions, the ethane flux through the external catalyst surface was at least four orders of magnitude lower than the molecular diffusion flux. So the external mass transfer resistance was assumed to be negligible. To calculate the activation energy, reaction rates were measured in the temperature range between 340 to 420°C. In between each measurement, the reactants gases (C_2H_6, H_2, and He) were replaced with H_2 to purge out the reactants remaining in the catalyst bed. The decrease of initial catalytic activity due to deactivation was about 1% of the initial activity. The reactant and product were analyzed by DS-6200 GC (Donam system, Korea) equipped with an FID detector. The Porapac Q column was used in ethane hydrogenolysis.

RESULTS

X-Ray Absorption Fine Structure (XAFS)

X-ray absorption near edge structure (XANES) was employed to investigate the electronic structure of platinum in every step of the catalyst preparation procedure, as shown in Fig. 2. These spectra have been plotted versus $E - E_o$ (total energy minus edge energy). The white line in the XANES spectra was changed for Pt/Al_2O_3 at each catalyst preparation step due to the change of the multiple scattering. The amplitude of the white line was considerably decreased by the reduction treatment, indicating the reduction from Pt^{4+} to Pt^0.

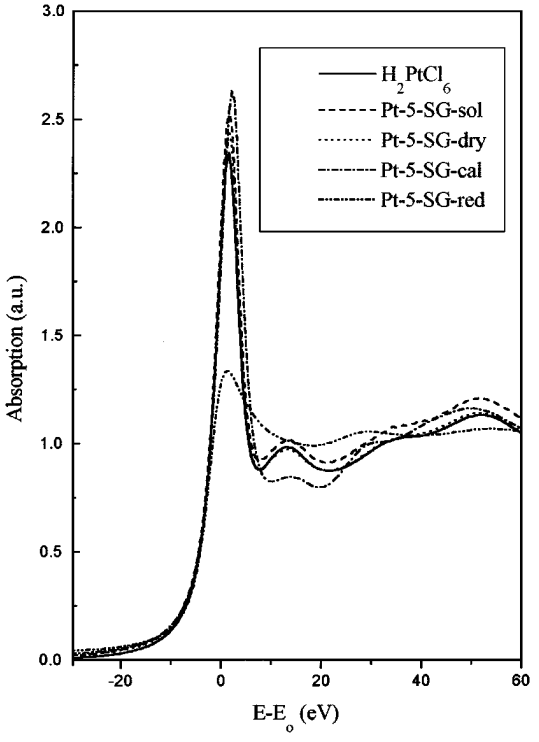

FIG. 2. XANES spectra above Pt L_{III} edge of 5% Pt/γ-Al_2O_3 at each preparation step.

The extended X-ray absorption fine structure (EXAFS) oscillation ($\chi(k)$) was multiplied by the wave vector cube (k^3) after background removal and normalization. The background was removed with an *r*-space technique that optimized low-*r* background components in the Fourier transform (FT) through comparison with a standard XAFS generated using FEFF6 code (24, 25).

The structural parameters obtained from the curve-fitting of FT data are listed in Table 1. There was no distinct change

TABLE 1

Structural Parameters Obtained from EXAFS Curve Fit for 5% Pt/γ-Al_2O_3 Catalyst at Each Preparation Step

Samples	Pair	CN[a]	R (Å)[b]	σ^2 (Å^2)[c]
H_2PtCl_6	Pt–Cl	6.1	2.31	0.0023
Pt-5-SG-sol	Pt–Cl	5.7	2.35	0.0023
Pt-5-SG-dry	Pt–Cl	5.7	2.33	0.0026
Pt-5-SG-cal	Pt–O	5.9	2.00	0.0047
Pt-5-SG-red	Pt–Pt	6.4	2.71	0.0114
	Pt–O	2.0	2.41	0.0139
Pt-5-SG-sin	Pt–Pt	8.8	2.77	0.0056
Pt-5-IM-cal	Pt–O	6.7	2.01	0.0068
Pt-5-IM-red	Pt–Pt	6.1	2.71	0.0092
Pt-5-IM-sin	Pt–Pt	9.6	2.77	0.0052

[a] Coordination number (±0.5).
[b] Bond distance (±0.01 Å).
[c] Debye–Waller factor (±5).

in coordination number (CN) of Pt–Cl between H_2PtCl_6 and dried Pt/Al_2O_3 sample (Pt-5-SG-dry). Upon calcination at 773 K, the platinum was converted to platinum oxide. The platinum oxide was reduced by hydrogen and formed small platinum particles consisting of 20 atoms, ca 1 nm. The size was estimated from the Pt–Pt CN.

The near edge spectrum of the Pt-5-SG-red the Pt L_{III} edge is compared with that of the Pt-5-IM-red in Fig. 3. The amplitude of white line in the sol–gel catalyst is higher than that of the impregnated catalyst, indicating a metal–support interaction.

EXAFS data in *k*- and *r*-space of both sol–gel catalysts and impregnated catalyst are shown in Fig. 4, where Fourier transformation was performed using the data in the range of $3.0 \leq k \leq 14.0$ Å^{-1}. The oscillations in *k* space of both catalysts are slightly different amplitude and shape. Table 1 shows that the Pt–Pt CN of 5% Pt/γ-Al_2O_3 sol–gel sample, 6.4, was almost the same as that of the impregnated catalyst, 6.1. The particle size in the both catalysts is the same regardless of the preparation method. However, in the sol–gel catalyst, the Pt–O contribution in the EXAFS is present at 2.41 Å, consistent with the metal–support interaction (27, 28).

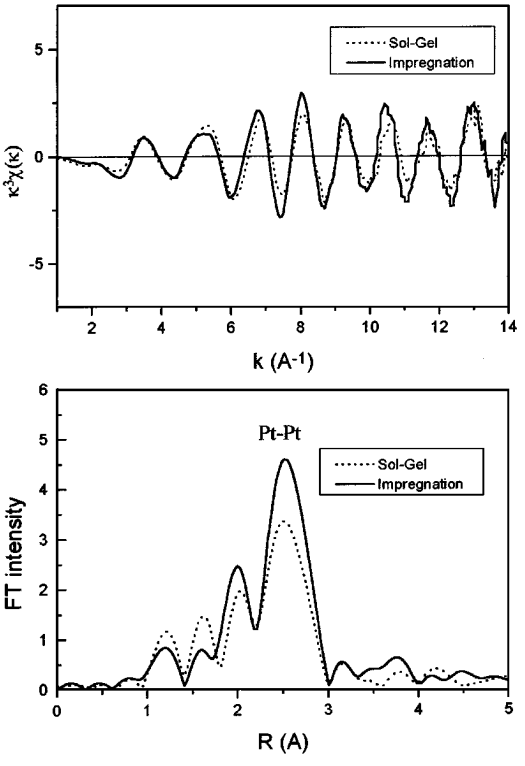

FIG. 4. k^3-weighted EXAFS oscillation for reduced 5% Pt/γ-Al_2O_3 samples (upper part) and Fourier transform in *r*-space (lower part).

BET Surface Area and Pore Size Distribution

Either the BET or the Langmuir equation was used for surface area calculations depending on which was appropriate for the given data. Nitrogen desorption was used to calculate mesopore size distribution by applying a method based on the BJH (Barrett, Joyner, and Hallender) method (36). The micropore volume was obtained using the *t*-plot analysis method. The adsorption–desorption isotherms of blank alumina, sol–gel catalyst, and impregnated catalyst are shown in Fig. 5. No isotherms similar to the so-called Type I isotherm were obtained, indicating that there is no significant fraction of small pores in these samples. For the Pt-5-SG-red, the micropore volume was small (0.012 and 0.0075 ml/g, respectively) while the mesopore volume was 0.18 ml/g. The total surface area of meso- and macropores was 218 m^2/g. Because the total surface area of the micropores was only 22 m^2/g, a significant fraction of the surface area was in the mesopore.

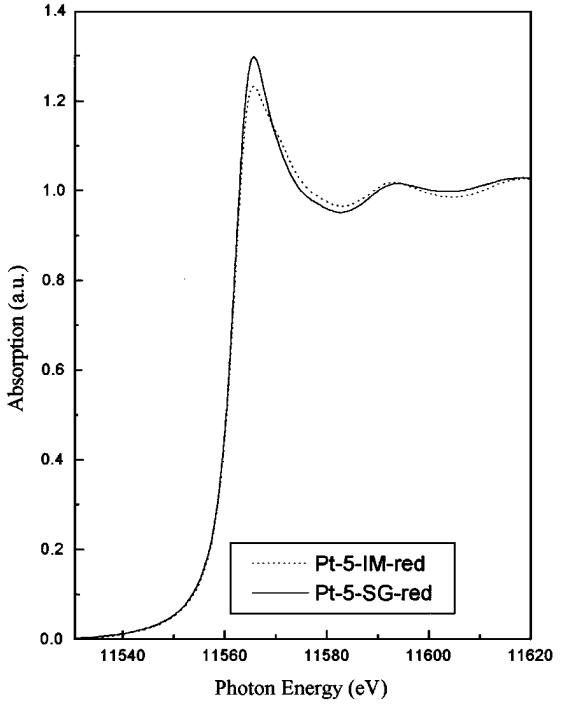

FIG. 3. XANES spectra above Pt L_{III} edge of 5% Pt/γ-Al_2O_3 reduced at 400°C for 2 h.

The pore size distributions of pure alumina and Pt-loaded alumina samples are shown in Fig. 6. There was no significant change in pore size distribution between sol–gel catalyst and impregnated catalyst. The pore structure of impregnated catalyst was almost the same as that of blank alumina prepared by the sol–gel method without the addition of Pt precursor.

Table 2 shows the BET surface, pore volume, and average pore size of γ-Al_2O_3 calcined at 773 K for 5 h and Pt/γ-Al_2O_3 reduced at 673 K for 2 h. The BET surface area and pore volume of the sol–gel catalyst were also found to

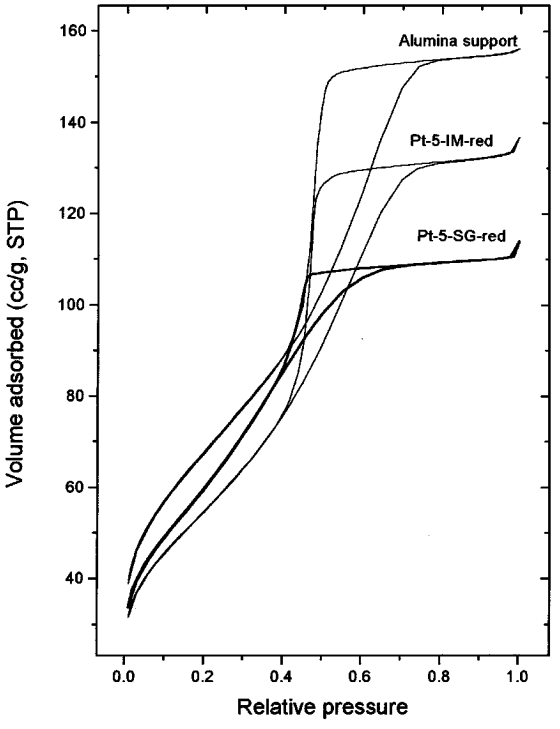

FIG. 5. Adsorption–desorption isotherms for blank alumina, sol–gel catalyst, and impregnated catalyst.

be almost the same as that prepared by the impregnation method. It is noteworthy that the pore structure does not change with the preparation method, either by addition of $H_2PtCl_6 \cdot xH_2O$ to alumina sol, or by impregnation of Pt precursor into calcined alumina. It is peculiar that the microporous structure was developed on the sol–gel catalyst, as shown in Fig. 6b. However, the presence of the micropore

TABLE 2

BET Surface Area, Pore Volume, and Pore Size of Pt/γ-Al_2O_3 Catalysts

Sample	BET surface area (m^2/g)	Pore volume (cc/g)	Pore size (nm)
γ-Al_2O_3	246	0.24	3.7
Pt-1-SG-red	225	—	—
Pt-1-IM-red	219	—	—
Pt-5-SG-red	218	0.18	2.8
Pt-5-IM-red	199	0.21	3.3

does not significantly change the average pore size distribution and surface area of the sol–gel catalyst, compared with the impregnated catalyst.

Hydrogen Chemisorption

Table 3 summarizes the result of the metal loading and hydrogen chemisorption for Pt/γ-Al_2O_3 samples. The hydrogen uptake for sol–gel catalyst was lower than that of impregnated catalyst. The hydrogen chemisorption on sol–gel samples was around 70–80% of that for the corresponding impregnated samples.

Catalytic Activity

The turnover frequency (TOF) of ethane hydrogenolysis reaction over Pt/γ-Al_2O_3 catalysts was calculated by the expression

$$\mathrm{TOF} = \boldsymbol{n}/\boldsymbol{S},$$

where $\boldsymbol{n}$ is the number of ethane molecules reacted per unit time and $\boldsymbol{S}$ is the number of surface metal sites measured by the hydrogen chemisorption as shown in Table 2. The

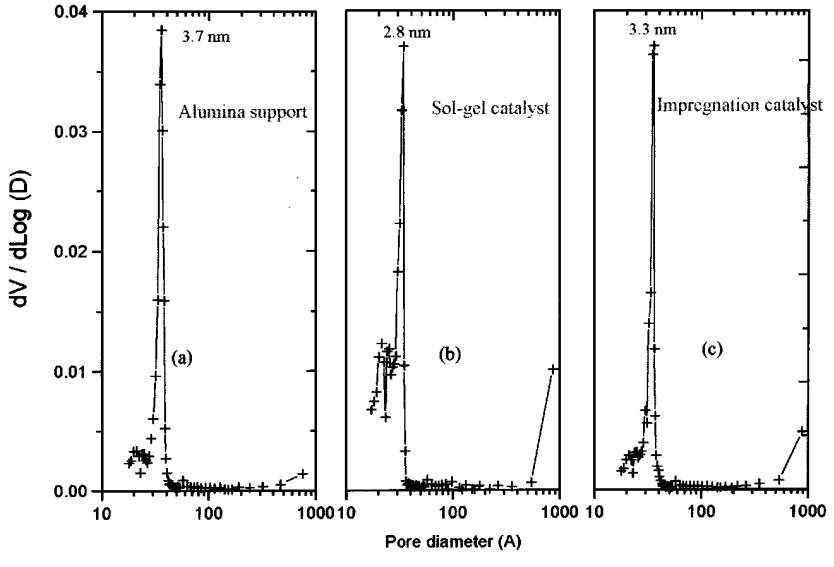

FIG. 6. Pore size distribution obtained from the nitrogen desorption at 77 K: (a) γ-Al_2O_3, (b) Pt-5-SG-red, and (c) Pt-5-IM-red.

TABLE 3

Hydrogen Uptakes for Pt/γ-Al_2O_3 Catalysts Obtained from the Hydrogen Chemisorption and H_2–O_2 Titration Method

Samples	Metal content (wt%)	H_2 uptake (μmol/gcat)	H/Pt
Pt-1-SG-red[a]	0.86	23.9	1.08
Pt-1-IM-red[a]	1.03	35.0	1.32
Pt-5-SG-red[b]	4.24	63.1	0.58
Pt-5-IM-red[b]	4.33	88.8	0.80

[a] Based on hydrogen back-sorption.
[b] Based on hydrogen–oxygen titration.

TABLE 4

The Activation Energy of Ethane Hydrogenolysis Reaction

Reference	Temperature range (°C)	Ed (kcal/mol)	Reaction conditions
This work	340–395	29	Pt-5-SG-red $P_{H_2} = 0.33$ atm, $P_{C_2H_6} = 0.060$ atm
This work	340–395	28	Pt-5-IM-red $P_{H_2} = 0.33$ atm, $P_{C_2H_6} = 0.060$ atm
This work	388–419	36	Pt-1-SG-red $P_{H_2} = 0.33$ atm, $P_{C_2H_6} = 0.060$ atm
This work	390–419	36	Pt-1-IM-red $P_{H_2} = 0.33$ atm, $P_{C_2H_6} = 0.060$ atm
Sinfelt *et al.* (35)	343–401	31	0.60% Pt/γ-Al_2O_3 $P_{H_2} = 0.20$ atm, $P_{C_2H_6} = 0.030$ atm

TOFs of ethane hydrogenolysis reaction over 1 and 5% Pt/γ-Al_2O_3 catalysts are shown in Fig. 7. The TOFs of sol–gel catalysts are lower than those of sol–gel catalysts in the reduced state throughout the temperature range. As the metal loading changes from 5 to 1%, the difference in TOFs between sol–gel and impregnated catalyst increases. The TOF of Pt-5-SG-red is about 1.5 times lower than that of Pt-5-IM-red. Even for the Pt-1-SG-red catalyst, the TOF is much smaller by one order of magnitude than that for impregnation catalyst. However, catalytic behaviors of the sintered catalysts were different. The sintered sol–gel catalyst showed more activity than that of the impregnated catalyst. The TOF of Pt-5-SG-sin was higher than that of the corresponding impregnated catalyst, as shown in Fig. 7b.

The activation energies of present catalysts are listed in Table 4 and are compared with one other literature report.

Thermal Stability

XRD patterns of 1% Pt/γ-Al_2O_3, obtained before and after sintering at 873 K for 20 h under air flow, are shown in Fig. 8. The peak assigned to Pt metals appeared at 38° in both impregnated and sol–gel catalysts after the heat treatment. The intensity of the Pt metal peak for impregnation catalyst was much higher than that for sol–gel catalyst.

TEM micrographs of the Pt/γ-Al_2O_3 samples after sintering are shown in Fig. 9. The Pt particles were not detectable before the sintering for both the sol–gel and impregnated catalysts, indicating that Pt particles were very small for both catalysts. Large Pt metal particles were formed in

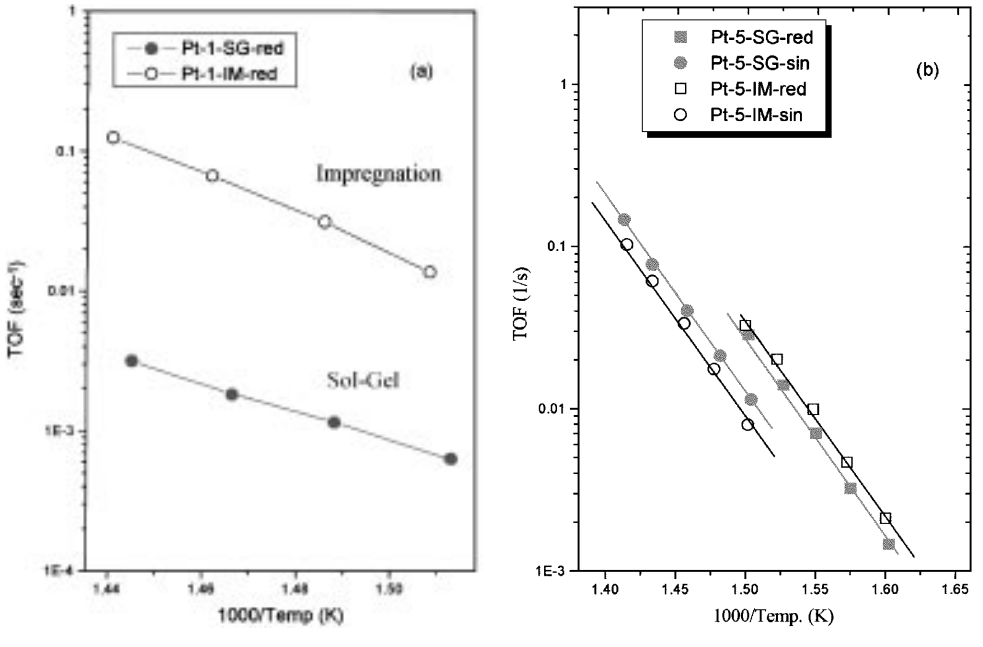

FIG. 7. Catalytic activity for ethane hydrogenolysis reaction over 1% (a) and 5% (b) Pt/γ-Al_2O_3 catalysts.

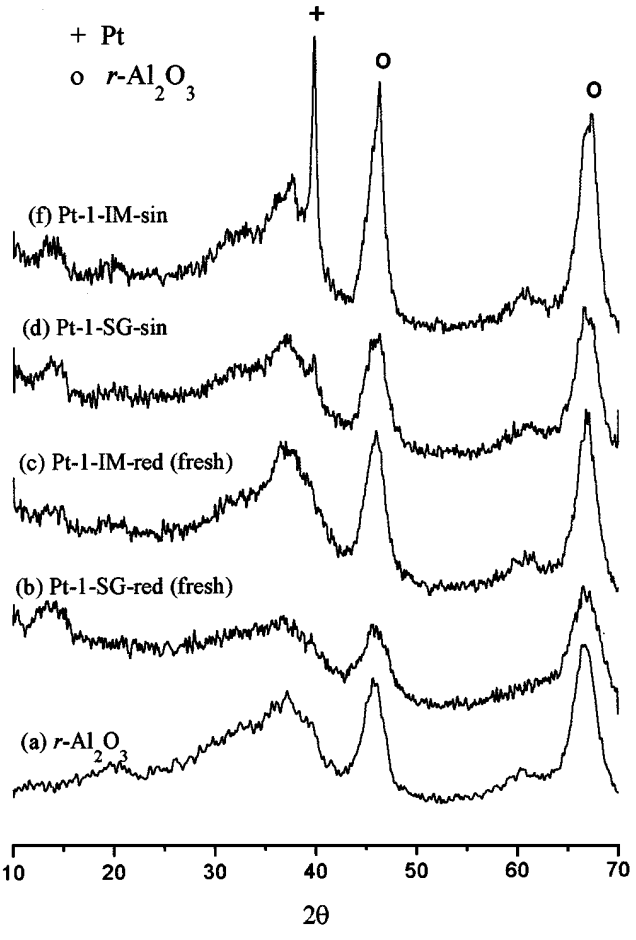

FIG. 8. XRD patterns of 1% Pt/Al_2O_3 catalyst before and after sintering at 873 K for 20 h followed by reduction at 873 K for 2 h.

the impregnated catalyst after sintering treatment, but not on the sol–gel catalyst, which indicated that the sol–gel catalyst was more resistant to sintering under high temperature. The increased resistance for the sintering was due to the presence of Pt–O coordination in the sol–gel catalyst.

DISCUSSION

The average number (n_{Pt}) of Pt atoms per particle was estimated from the correlation curve between the theoretical coordination number and the number of Pt atoms per particles by assuming that the particles were spherical shaped and closely packed *fcc* (29). As shown in Table 1, the Pt–Pt CN was about 6.0 for both the sol–gel and impregnated catalysts. From the correlation curve, the n_{Pt} was calculated to be 20. This indicates that the average particle size for the catalysts is less than 1 nm.

$Pt/\gamma\text{-}Al_2O_3$ catalysts prepared by sol–gel method had smaller hydrogen chemisorption than those prepared by impregnation method. This result suggests that 20–30% less platinum sites were accessible for hydrogen chemisorption and Pt particles in the sol–gel catalyst were surrounded or buried by alumina, consistent with Lopez *et al.* (13). They prepared a Pt/SiO_2 catalyst by adding Pt salts to the TEOS before gelling and measured the Pt particle size with hydrogen chemisorption and TEM. The discrepancy in Pt particle size measured by the two different methods was attributed to the partially buried Pt particles into the surface, as shown in Fig. 10. The Pt particle size measured by hydrogen chemisorption was apparently larger than that measured by TEM.

In ethane hydrogenolysis, the reaction intermediate (C_2H_x) requires a site comprising an ensemble of multiple surface platinum atoms (30–32). Therefore, the TOF in ethane hydrogenolysis generally increases with metal particle size, because larger metal particles will have more ensembles of multiple Pt atoms than smaller particles. The $Pt/\gamma\text{-}Al_2O_3$ sol–gel catalyst shows lower activity than the impregnated catalyst, indicating that sol–gel catalysts have a limited number of ensembles due to blocking of the Pt active sites by alumina support. This fact supports the conclusion that Pt particles are partially surrounded by the alumina support. Mizushima and Hori found similar catalytic behavior for the methane combustion reaction on Pt/Al_2O_3 aerogel catalyst (4). They reported that the Pt/Al_2O_3 aerogel has a more uniform distribution and higher dispersion (6 nm by TEM) than that of a conventional catalyst (15 nm), while its conversion of methane combustion was lower than that of impregnated catalyst. They explained that the lower catalytic activity of aerogel catalysts was due to the fact that some Pt particles were surrounded by alumina and were unable to react with the methane.

The durability for sintering confirmed that the Pt particles were strongly interacting with the alumina surface in the sol–gel catalyst, consistent with the results of the EXAFS. The strong attachment of Pt particles to the support restricts the agglomeration of Pt particles in air and high temperature.

The catalytic activity can also be decreased due to a partially reduced Pt surface for the sol–gel catalyst. Laiyuan *et al.* have reported that the Pt/Al_2O_3 catalysts, prepared by impregnating the $\gamma\text{-}Al_2O_3$ with H_2PtCl_6, have two reduction peaks at about 573 and 708 K (33). They explained that the peak at 573 K was due to the reduction of PtO_2 species and that the peak of 708 K was due to the reduction of platinum species which interact strongly with the support or to the reduction of a surface complex.

In the present work, the Pt/Al_2O_3 catalysts prepared by both the sol–gel and impregnation method were reduced at 673 K for 2 h under hydrogen. The result of XANES indicated that the Pt particle were reduced; Koningsberger and Gates suggested the long Pt–O bond in the range of 2.4–2.9 Å was evidence for the metal–support interaction (27, 34). Thus, the presence of the Pt–O bond at 2.4 Å in

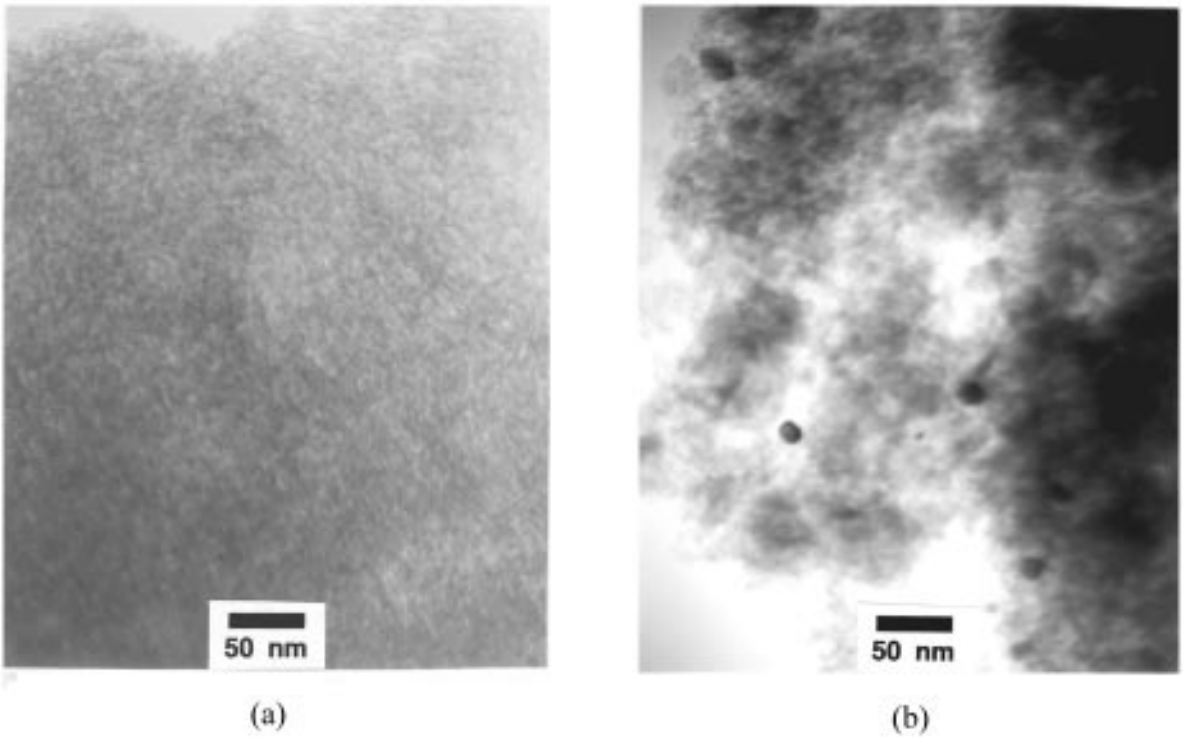

FIG. 9. TEM micrograph of 1% Pt/Al_2O_3 catalyst after sintering at 873 K for 20 h: (a) Pt-1-SG-sin; (b) Pt-1-IM-sin.

the sol–gel catalyst would indicate a stronger metal–support interaction, compared with that of the impregnated catalyst.

CONCLUSIONS

An alumina supported platinum catalyst was prepared by sol–gel method. Its pore structure, metal dispersion, catalytic activity, and sintering resistivity were compared with those of impregnation catalysts. The $Pt/\gamma\text{-}Al_2O_3$ catalysts prepared by the addition of platinum precursor to the alumina sol had similar physical properties to the conventionally prepared impregnation catalyst. However, the Pt particles in the impregnated catalyst are present at the surface, while in the sol–gel catalyst, the Pt particles are partially buried in the alumina surface. Therefore, some of the Pt surface sites are not accessible by molecules such as H_2, O_2, and C_2H_6. The $Pt/\gamma\text{-}Al_2O_3$ catalysts prepared by sol–gel method show higher thermal stability of metal particles than the conventional impregnation catalyst, because the exposed Pt metal particles are strongly anchored into the alumina support by metal–support oxygen bonding.

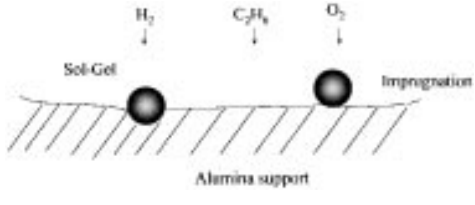

FIG. 10. A schematic diagram of configurations of metal particles with respect to the support.

ACKNOWLEDGMENTS

This research was supported by the Research Center for Catalytic Technology of Pohang Institute of Science and Technology (1996). The authors are grateful to the Photon Factory in Tsukuba, Japan (Proposal 95G210).

REFERENCES

1. Ward, D. A., and Ko, E. I., *Ind. Eng. Chem. Res.* **34**, 421 (1995).
2. Cauqui, M. A., and Rodriguez-Izquierdo, J. M., *J. Non-Cryst. Solids* **147&148**, 724 (1992).
3. Pajonk, G. M., *Appl. Catal.* **72**, 217 (1991).
4. Mizushima, Y., and Hori, M., *Appl. Catal.* **88**, 137 (1992).
5. Balakrishnan, K., and Gonzalez, R. D., *J. Catal.* **144**, 395 (1993).
6. Armor, J. N., Carlson, E. J., and Zambri, P. M., *Appl. Catal.* **19**, 339 (1985).
7. Zou, W., and Gonzalez, R. D., *Appl. Catal.* **102**, 181 (1993).
8. Zou, W., and Gonzalez, R. D., *Appl. Catal.* **126**, 351 (1995).
9. Lopez, T., Herrera, L., Gomez, R., Zou, W., Robinson, K., and Gonzalez, R. D., *J. Catal.* **136**, 621 (1992).
10. Lopez, T., Bosch, P., Asomoza, M., and Gomez, R., *J. Catal.* **133**, 247 (1992).
11. Lopez, T., Gomez, R., Novaro, O., Ramirez-Solis, A., Sanchez-Mora, E., Castillo, S., Poulain, E., and Martinez-Magadan, J. M., *J. Catal.* **141**, 114 (1993).
12. Lopez, T., Lopez-Gaona, A., and Gomez, R., *Langmuir* **6**, 1343 (1990).

13. Bosch, P., Lopez, T., Lara, V.-H., and Gomez, R., *J. Mol. Catal.* **80**, 299 (1993).
14. Azomoza, M., Lopez, T., Gomez, R., and Gonzalez, R. D., *Catal. Today* **15**, 547 (1992).
15. Lopez, T., Romero, A., and Gomez, R., *J. Non-Cryst. Solids* **127,** 105 (1991).
16. Lopez, T., Bosch, P., Moran, M., and Gomez, R., *J. Phys. Chem.* **97,** 1671 (1993).
17. Lopez, T., Lopez-Gaona, A., and Gomez, R., *J. Non-Cryst. Solids* **110**, 170 (1989).
18. Lopez, T., Moran, M., Navarrete, L., Herrera, L., and Gomez, R., *J. Non-Cryst. Solids* **147&148**, 753 (1992).
19. Lopez, T., Bosch, P., Navarrete, M., Asomoza, J., and Gomez, R., *J. Sol–Gel Sci. and Tech.* **1**, 193 (1994).
20. Lopez, T., Villar, M., and Gomez, R., *J. Phys. Chem.* **95**, 1690 (1991).
21. Zou, W., and Gonzalez, R. D., Lopez, T., and Gomez, R., *Mat. Lett.* **24**, 35 (1995).
22. Zou, W., and Gonzalez, R. D., *J. Catal.* **152**, 291 (1995).
23. Frenkel, A. I., Stern, E. A., Qian, M., and Newville, M., *Phys. Rev. B* **48**, 12449 (1993).
24. Newville, M., Livins, P., Yacoby, Y., Rehr, J. J., and Stern, E. A., *Phys. Rev. B* **47**, 14126 (1993).
25. Rehr, J. J., Albers, R. C., and Zabinski, S. I., *Phys. Rev. Lett.* **69**, 3397 (1992).
26. Benson, J. E., and Boudart, M., *J. Catal.* **4**, 704 (1965).
27. Koningsberger, D. C., and Gates, B. C., *Catal. Lett.* **14**, 271 (1992).
28. Cho, S. J., Ahn, W.-S., Hong, S. B., and Ryoo, R., *J. Phys. Chem.* **100**, 4996 (1996).
29. Kampers, F. W. H., Engelen, C. W. R., Van Hooff, J. H. C., and Koningsberger, D. C., *J. Phys. Chem.* **94**, 8574 (1990).
30. Sinfelt, J. H., *Adv. Catal.* **23** (1973).
31. Sinfelt, J. H., and Yates, D. J. C., *J. Catal.* **8**, 82 (1967).
32. Sinfelt, J. H., *Catal. Lett.* **9**, 159 (1991).
33. Laiyuan, C., Yueqin, N., Jingling, Z., Liwu, L., Xihui, L., and Sen, C., *J. Catal.* **145**, 132 (1994).
34. Munoz-Paez, A., and Koningsberger, D. C., *J. Phys. Chem.* **99**, 4193 (1995).
35. Sinfelt, J. H., *J. Phys. Chem.* **68**, 344 (1964).
36. Instruction Manual for Micromeritics ASAP 2400, Micromeritics, Norcross GA, (1991) U.S.A.